Automatic Markov Random Field Segmentation of Susceptibility-Weighted MR Venography

Silvain Bériault(✉), Marika Archambault-Wallenburg, Abbas F. Sadikot, D. Louis Collins, and G. Bruce Pike

McConnell Brain Imaging Centre, Montreal Neurological Institute, 3801 University Street, Montreal, QC H3A 2B4, Canada
silvain.beriault@mail.mcgill.ca

Abstract. Patient-specific cerebrovascular modeling provides essential information to facilitate the identification of vessel-free trajectories in functional neurosurgery. However, standard gadolinium models used clinically are often incomplete due to the extent of manual labor required to segment the vessels and because gadolinium contrast decreases rapidly with vessel size. In this work, we propose an automatic method, based on the Markov Random Field (MRF) theory, to segment venous blood vessels from dense susceptibility-weighted imaging (SWI) venography datasets. Unlike conventional isotropic auto-logistic MRF, our MRF design anisotropically favors the neighboring influence of voxels classified as "vessels" to better preserve thin vessels imaged by SWI. Results show that MRF segmentation of deep veins compares well with standard scale-space vesselness analysis. Most importantly, we demonstrate automatic segmentation of superficial veins on SWI and creation of denser 3D vascular models that may improve clinical gadolinium-based models.

Keywords: MR venography · Susceptibility-weighted imaging · Markov random fields · Image-guided neurosurgery · Deep brain stimulation

1 Introduction

With a reported incidence rate as high as 5 % in recent literature [1], hemorrhagic complications pose a high risk of devastating post-operative neurological deficits in functional image-guided neurosurgery. During the pre-surgical planning stage, patient-specific 3D models of the cerebral vasculature are commonly created to guide the neurosurgeon in identifying vessel-free insertion trajectories. In many centers, this task consists of segmenting the cerebral vasculature, either manually or semi-automatically, from a gadolinium-enhanced T1w MRI dataset. However, these models are often incomplete due to the extent of manual labor required and because gadolinium enhancement decreases rapidly in smaller vessels. This work describes a new framework for the automatic segmentation of susceptibility-weighed imaging (SWI) venography datasets.

M. Erdt et al. (Eds.): CLIP 2013, LNCS 8361, pp. 39–47, 2014.
DOI: 10.1007/978-3-319-05666-1_6,

Susceptibility weighted imaging (SWI) [2] is a relatively new T2*-weighted gradient echo MRI technique that exploits both the magnitude and phase of the complex MRI signal to increase sensitivity to deoxygenated (venous) blood and to deep brain structures rich in iron content. SWI already provides useful information in a variety of clinical applications including traumatic brain injury, vascular malformations, strokes and neurodegenerative disorders [3]. However, for neurosurgical planning purposes, the reversed vessel contrast imaged by SWI poses new segmentation challenges.

Although several automatic vessel segmentation methods have been proposed in the computer-vision literature [4], techniques that were successfully applied to SWI most often fall under the categories of scale-space analysis or statistical models [5]. Multi-scale "vesselness" filtering methods [6, 7] were shown to produce acceptable results on SWI for deep veins [5, 8], but not for superficial veins [9]. This is due to the absence of a fully defined "tubular-like" 3D contrast between surface veins and surrounding skull. However, surface vein avoidance is essential in functional neurosurgery [10]. Alternatively, statistical methods using local intensity thresholds were investigated [5] but they tend to necessitate post-processing to improve the results.

This paper presents a new statistical segmentation framework based on the Markov Random Field (MRF) theory, and extends the previous work of Hassouna *et al.* [11] originally applied to time-of-flight (TOF) angiography. MRFs are a key step in many segmentation applications to incorporate spatial dependencies among neighboring voxels. For simplicity, the influence of neighboring voxels is often considered isotropic. While this assumption holds for blob-like regions and may hold for the segmentation of major arteries imaged by TOF, an isotropic assumption does not suffice for preserving thinner vessels imaged by SWI. In this work, we describe the implementation of an anisotropic MRF with spatially varying neighborhood influence.

2 Methods

SWI segmentation is implemented as a labeling problem. Each site in the dataset (i.e. the voxels) is labeled as either vessel (V) or tissue (T). Let $S = \{1, \ldots, N\}$ denote the sites and $L = \{V, T\}$ the possible labels. Let $Y = \{y_1, \ldots y_2, \ldots, y_N\}$, $X = \{x_1, \ldots x_2, \ldots, x_N\}$ denote respectively the observed voxel intensity and the output classification at each site in S. The segmentation is performed in three steps:

1. An initial labeling X is found based on the observed intensities Y by expectation maximization (EM).
2. This initial segmentation is further refined with an auto-logistic MRF model to integrate spatial dependencies about the classification of neighboring sites.
3. A skull stripping procedure is computed to distinguish between surface veins and dark-appearing skull.

2.1 Statistical Model

Vessel and brain tissue classes are modeled as a mixture of two normal distributions with parameters $\theta_l = \{w_l, u_l, \sigma_l^2\}$, $l \in \{V, T\}$, where w_l represents the proportions between the two classes. An EM algorithm is applied iteratively for finding the maximum-likelihood estimate of the parameters $\theta_v = \{w_v, u_v, \sigma_v^2\}$and $\theta_T = \{w_T, u_T, \sigma_T^2\}$. During the E step, the model parameters $\{\theta_v, \theta_T\}$are held fixed and the posterior probability $f^k(l|y_i)$ of voxel i belonging to class l given its intensity y_i is calculated. During the M step, the model parameters $\{\theta_v, \theta_T\}$ are updated for the next iteration $(k + 1)$. The EM algorithm is applied to brain voxels only (an approximate brain mask is estimated using a co-registered T1w dataset). Proportions w_v^0 and w_T^0 are initialized to 0.05 and 0.95 since blood vessels occupy less than 5 % of the whole brain volume. A simple Otsu threshold is sufficient to estimate initial $\{\mu_l^0, \sigma_l^0\}$ values for the V and T classes. Upon EM convergence, the labeling X for all sites in S is assigned to maximize $f(l|y_i)$:

$$x_i = \arg\max_{l\in\{V,T\}} f(l|y_i), \forall i \in S, \tag{1}$$

$$\text{with } f(l|y_i) = \frac{w_l f(y_i|l)}{\sum_{j=1}^{L} w_j f(y_i|l)}, \text{ and } f(y_i|l) = \left(\frac{1}{\sqrt{2\pi\sigma_l^2}}\right)\exp\left(\frac{-(y_i-\mu_l)^2}{\sqrt{2\sigma_l^2}}\right). \tag{2}$$

2.2 Anisotropic Auto-logistic MRF Model

We implemented an auto-logistic MRF model to refine the initial EM classification by taking into account the classification of neighboring voxels $x_j \in \eta_i$. In our case, η_i is defined to contain all sites x_j within a $3 \times 3 \times 3$ neighborhood of x_i. In the MRF theory, the unknown classification X is modeled as a random process that, according to the Hammersley-Clifford theorem, must obey a Gibbs distribution of the form: $P(X) = Z^{-1}\exp(-U(X))$, where $Z = \sum \exp(-U(X))$ is a normalizing constant called the partition function containing all possible configurations of X. Clearly, exact computation of the partition function on 3D volumetric data is an intractable combinatorial problem. However, it can be avoided if all parameters defining $U(X)$ are properly estimated. In the auto-logistic MRF case, the energy function $U(X)$ is expressed as the sum of clique potential over all possible cliques (a clique is a subset of sites S). When only up to pair-site interactions are considered, the energy function takes the form:

$$U(X) = \sum\nolimits_{i\in S} \log(f(l|y_i)) + \sum\nolimits_{i\in S, j\in\eta_i} \beta_{ij} x_i x_j. \tag{3}$$

In (3), the first summation describes the unary association between voxel intensity y_i and class probabilities (see Sect. 2.1). The second summation describes the interaction between classification of voxel x_i and neighboring voxel x_j. β_{ij} is a clique potential parameter that encodes the specific interaction between each voxel pair. Similarity between neighboring voxels is favored when $\beta_{ij} > 0$. In the isotropic case, β_{ij} is either proportional to distance between sites i and j, or constant $(\beta_{ij} = \beta)$ to reduce the

number of estimated parameters. However, an isotropic MRF configuration applied to SWI will eliminate many thin veins simply because a majority of neighboring voxels would be classified as tissue. Instead, we implemented an anisotropic MRF where potential values β_{ij} are configured to favor the influence of neighboring voxels classified as vessel over those classified as tissue. Since the blood vessels in the dataset do not have the same orientation, the MRF is non-homogeneous, meaning the potential values β_{ij} vary with the spatial location of x_i. Since it is impractical to estimate β_{ij} for all possible voxel pairs in the dataset, we limit the potential β_{ij} to take a constant value of either β_V or β_T such that:

$$\beta_{ij} = \beta_{x_j} = \begin{cases} \beta_V, x_j = V \\ \beta_T, x_j = T \end{cases}. \tag{4}$$

When $\beta_V > \beta_T$, it takes fewer neighboring voxels x_j classified as V, within the local neighborhood η_i, to change the classification of voxel x_i from T to V then in the isotropic case. Reciprocally, it takes more voxels x_j classified as T to change the classification of voxel x_i from V to T then in the isotropic case. The relationship between β_V and β_T was estimated using the maximum pseudo-likelihood (PL) estimation method: $PL(X) = \prod_{x_i \in S} P\left(x_i | x_{\eta_i}\right)$, with

$$P\left(x_i | x_{\eta_i}\right) = \frac{\exp\left(\sum_{j \in \eta_i} \beta_{x_j} x_i x_j\right)}{1 + \exp\left(\sum_{j \in \eta_i} \beta_{x_j} x_j\right)}. \tag{5}$$

Thus a ratio β_V / β_T of 3.45 was estimated and used. With β_V and β_T terms described, the MRF is then solved using the iterated conditional mode method (ICM).

2.3 Surface Veins Extraction

Intensity-based classification does not permit separation between surface veins and skull, both labeled as V due to their similar intensities. As a final step, we model surface vasculature as concavities within the tissue surface. A skull-stripping mask that preserves brain tissue and surface veins is first computed via a binary majority filter applied iteratively to the T class. This filter approximates the convex hull of the T class. Then, vessel concavities are detected using a modified ball filter [12] that measures the local widening within a large neighborhood R_i for all surface voxels x_i classified as V.

$$E_R(i) = E_R^{'}(\mathrm{i}) + x_j \sum_{j \in R_i} E_R^{'}(\mathrm{j}), \text{ with } E_R^{'}(\mathrm{i}) = \sum_{j \in R_i} \chi\left(x_j\right), \chi\left(x_j\right) = \begin{cases} 0 x_j = T \\ 1 x_j = V \end{cases}. \tag{6}$$

Vessel concavities are detected by computing the ball measure twice, once with $R_i = sphere$ (a standard sphere shape centered at x_i) and once with $R_i = sheet$(a local 3D sheet-like shape of the brain surface also centered at x_i), to verify that $E_{R\,=\,ball}(i) \gg E_{R\,=\,sheet}(i)$.

3 Results and Discussion

SWI acquisitions were performed on a 3T Siemens TIM Trio scanner with a 32-channel head coil and we used a multi-echo acquisition strategy to increase signal-to-noise ratio [13]. Thus, magnitude and phase datasets were acquired from a 3D gradient echo sequence with transverse orientation, 0.5 × 0.5 × 1-mm resolution, 5 equally spaced echo times (TE) within the range 13–41 ms, a repetition time (TR) of 48 ms and a flip angle (α) of 17° for a total acquisition time of 10:24 min using GRAPPA acceleration (factor of 2). The first echo is fully flow compensated. The third and fifth echoes are flow compensated in the readout direction. Magnitude and phase images from each echo are combined by standard SWI reconstruction [2]. SWI reconstructed images are then averaged. The average dataset is resampled to 0.5-mm isotropic resolution, denoised with a non local means algorithm [14] and corrected for intensity non-uniformity [15].

3.1 Qualitative Evaluation

An example of MRF-based SWI segmentation is illustrated in Fig. 1. Figure 1a shows a 10-mm minimum intensity projection (mIP) slab of raw SWI data taken at the level of the lateral ventricles (deep venous system). Figure 1b show the MRF segmentation output and Fig. 1c shows the output of conventional multi-scale vesselness filtering using Frangi et al.'s [6] method with typical parameters: $\sigma = [0.5{-}2.5]$, $\Delta\sigma = 0.25$; $\alpha = 0.5$, $\beta = 0.5$, $\gamma =$ half the maximal Hessian norm. MRF segmentation provides a good fit to the raw SWI data, even for smaller lower-contrast septal and subependymal veins, and compares well with the vesselness output. Good agreement between the two vessel extraction techniques is observed up to voxels with very low vesselness value.

The key advantage of MRF segmentation over conventional vesselness filtering is illustrated in Fig. 2. Figure 2a shows a single SWI slice taken at the brain surface level. Figure 2b, c respectively show the output of EM (Sect. 2.1) and MRF/skull-stripping

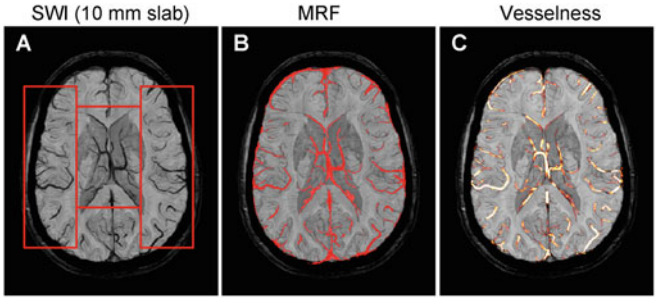

Fig. 1. Illustrative example of MRF-based segmentation at the level of the lateral ventricles. **(a)** A 10-mm minimum intensity projection (minIP) transverse slab from a raw SWI dataset **(b)** MRF segmentation. **(c)** Comparison to scale-space vesselness filtering. **(red boxes)** ROIs of the deep venous system and left/right sub-cortical veins used for validation of Sect. 3.2. (Color figure online)

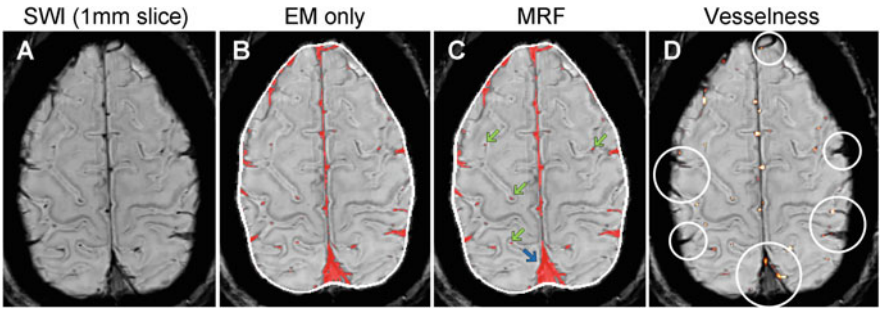

Fig. 2. Automatic segmentation of the surface vasculature. **(a)** A raw SWI slice at native resolution. **(b)** Output of EM segmentation. **(c)** Output of MRF segmentation and skull stripping (white contour) **(d)** Comparison with scale-space vesselness filtering. Vesselness filtering does not segment the SSS and the superficial cerebral veins (see white circles). **(blue arrow)** MRF regularization of SSS **(Green arrows)** Examples of thin, transversely oriented, vessels preserved during the MRF stage. (Color figure online)

(Sects. 2.2 and 2.3), in comparison to vesselness segmentation (Fig. 2d). At the brain surface, the MRF method achieves proper segmentation of the superior sagittal sinus (SSS) and of smaller superficial vessels. These vessels are not detected by vesselness filtering (see white circles) because they do not fit the tubular assumption. Furthermore, the SSS is particularly challenging to segment on SWI because of the lower contrast. Consequently, after the EM stage, several voxels belonging to the SSS are misclassified as "tissue". The integration of spatial dependencies (MRF stage) improves the SSS segmentation (see blue arrow). This regularization is achieved without eliminating thin, transversely oriented, vessels (see green arrows).

3.2 Quantitative Evaluation

We also quantitatively compared our MRF segmentation against 16 manually segmented SWI ROIs across 4 subjects. For each subject, these ROIs consist of one 10-mm mIP slab of the deep venous system (medial region of Fig. 1a), two 10-mm mIP slabs of the sub-cortical veins on the left and right hemispheres (e.g. lateral regions of Fig. 1a) and one whole slice taken at the brain surface level (e.g. Fig. 2). The kappa index was computed between the MRF and expert-based segmentations (MRF-manual kappa), and between conventional vesselness (υ) and expert-based segmentations (υ-manual kappa). Since the vesselness segmentation is non-binary, we considered the maximal υ-manual kappa index on a range of possible thresholds. Results of the comparison are shown in Table 1. For sub-cortical and deep veins, the MRF-manual kappa index falls in the range [0.70–0.90] with and median kappa of 0.86. Furthermore, the MRF-manual is higher then the maximal υ-manual kappa index for 11 out of 12 slabs. At brain surface, the maximal υ-manual kappa index drops to the range [0.36–0.56] while the MRF-manual kappa index stays in the range [0.77–0.84].

Table 1. Comparison between MRF-manual and maximal (υ)esselness-manual kappa indexes for 16 ROIs accross four subjects.

ROI	Subject 1		Subject 2		Subject 3		Subject 4	
	MRF	υ	MRF	υ	MRF	υ	MRF	υ
Deep venous system	0.85	0.76	0.85	0.79	0.83	0.76	0.80	0.77
Left subcortical veins	0.87	0.82	0.70	0.81	0.89	0.74	0.88	0.80
Right subcortical veins	0.90	0.81	0.86	0.79	0.86	0.78	0.86	0.81
Surface veins	**0.80**	**0.48**	**0.84**	**0.36**	**0.77**	**0.51**	**0.82**	**0.56**

3.3 Application to Neurosurgical Planning

As stated in introduction, patient-specific 3D models of the cerebral vasculature (and surface vasculature in particular) are often used to identify vessel-free insertion trajectories in minimally invasive functional neurosurgery. Figure 3 shows some examples of cerebrovascular models created from SWI and Gadolinium-enhanced MRI. Four patients who underwent deep brain stimulation (DBS) surgery were scanned with both MRI protocols. The SWI datasets (top row) were segmented using the automatic MRF method. The gadolinium-enhanced datasets (bottom row) were manually segmented on the Medtronic StealthStation® platform by the clinical neuronavigation team and used for planning the actual DBS intervention. The manually processed clinical models may qualitatively appear smoother but are limited to the main vasculature only and the clinical model for subject 4 is particularly incomplete. Automatically processed SWI datasets result in denser models of the surface veins and more side branches can be observed.

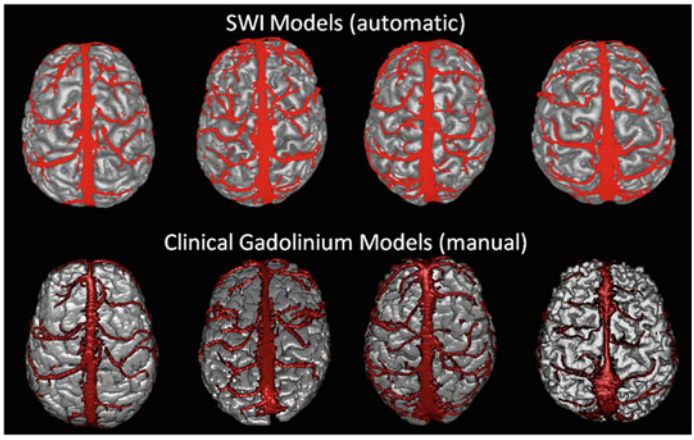

Fig. 3 (top row) Automatic reconstruction of surface veins by MRF on SWI. (bottom row) Comparison to manual segmentation on gadolinium enhanced MRI, created using the Medtronic StealthStation® platform, and used clinically for DBS planning.

4 Conclusion

Avoiding the cerebral vasculature is essential in functional neurosurgery to minimize risks of post-operative neurological deficits. Due to the high inter-subject variability, the cerebral vasculature must be imaged and segmented for each patient individually. For this purpose, SWI provides more detailed imaging of cerebral veins in comparison to conventional gadolinium protocols without requiring injection of contrast agent. However, automatic segmentation of SWI vasculature is challenging, especially at brain surface, due to the reversed venous contrast. In this work, we presented an anisotropic MRF framework to segment both sub-cortical and the surface vasculature on SWI data. To our knowledge, this is the first method that applies MRF for SWI segmentation and, most importantly, to demonstrate adequate SWI segmentation of the surface vasculature. Future work will concentrate on extending this MRF approach for segmenting SWI veins at the basal ganglia level and distinguishing them from other hypo-intense (iron-rich) nuclei present in this area.

References

1. Zrinzo, L., Foltynie, T., Limousin, P., Hariz, M.I.: Reducing hemorrhagic complications in functional neurosurgery: a large case series and systematic literature review. J. Neurosurg. **116**, 84–94 (2012)
2. Haacke, E.M., Xu, Y., Cheng, Y.C., Reichenbach, J.R.: Susceptibility weighted imaging (SWI). Magn. Reson. Med. **52**, 612–618 (2004)
3. Mittal, S., Wu, Z., Neelavalli, J., Haacke, E.M.: Susceptibility-weighted imaging: technical aspects and clinical applications, part 2. AJNR Am. J. Neuroradiol. **30**, 232–252 (2009)
4. Lesage, D., Angelini, E.D., Bloch, I., Funka-Lea, G.: A review of 3D vessel lumen segmentation techniques: models, features and extraction schemes. Med. Image Anal. **13**, 819–845 (2009)
5. Haacke, E.M., Reichenbach, J.R.: Susceptibility weighted imaging in MRI: basic concepts and clinical applications. Wiley-Blackwell, Hoboken (2011)
6. Frangi, A., Niessen, W., Vincken, K., Viergever, M.: Multiscale vessel enhancement filtering. In: Wells, W.M., Colchester, A.C.F., Delp, S.L. (eds.) MICCAI 1998. LNCS, vol. 1496, pp. 130–137. Springer, Heidelberg (1998)
7. Manniesing, R., Viergever, M.A., Niessen, W.J.: Vessel enhancing diffusion: a scale space representation of vessel structures. Med. Image Anal. **10**, 815–825 (2006)
8. Koopmans, P.J., Manniesing, R., Niessen, W.J., Viergever, M.A., Barth, M.: MR venography of the human brain using susceptibility weighted imaging at very high field strength. MAGMA **21**, 149–158 (2008)
9. Beriault, S., Subaie, F.A., Collins, D.L., Sadikot, A.F., Pike, G.B.: A multi-modal approach to computer-assisted deep brain stimulation trajectory planning. Int. J. Comput. Assist. Radiol. Surg. **7**, 687–704 (2012)
10. Benabid, A.L., Chabardes, S., Mitrofanis, J., Pollak, P.: Deep brain stimulation of the subthalamic nucleus for the treatment of Parkinson's disease. Lancet Neurol. **8**, 67–81 (2009)
11. Hassouna, M.S., Farag, A.A., Hushek, S., Moriarty, T.: Cerebrovascular segmentation from TOF using stochastic models. Med. Image Anal. **10**, 2–18 (2006)

12. Nain, D., Yezzi, A., Turk, G.: Vessel segmentation using a shape driven flow. In: Barillot, C., Haynor, D.R., Hellier, P. (eds.) MICCAI 2004. LNCS, vol. 3216, pp. 51–59. Springer, Heidelberg (2004)
13. Denk, C., Rauscher, A.: Susceptibility weighted imaging with multiple echoes. J. Magn. Reson. Imag. **31**, 185–191 (2010)
14. Coupe, P., Yger, P., Prima, S., Hellier, P., Kervrann, C., Barillot, C.: An optimized blockwise nonlocal means denoising filter for 3-D magnetic resonance images. IEEE Trans. Med. Imag. **27**, 425–441 (2008)
15. Sled, J.G., Zijdenbos, A.P., Evans, A.C.: A nonparametric method for automatic correction of intensity nonuniformity in MRI data. IEEE Trans. Med. Imag. **17**, 87–97 (1998)